Design of Experimental Setup for Studies of a Wind Energy Conversion System Using a Power Split Device in Industrial Wind Turbines

E. D. B. Møgelbjerg, E. B. Riisager, F. L. Nielsen, M. M. Lau, N. P. K. Hjortshøj, N. L. Christensen, V. H. Olesen

Department of Materials and Production, Aalborg University
Fibigerstraede 16, DK-9220 Aalborg East, Denmark
Email: {emagel19, eriisa19, flni19, mlau19, nhjort19, nchr19, volese19}@student.aau.dk,
Web page: http://www.mechman.mp.aau.dk/

Abstract
This paper investigates a concept proposed by [1], that uses a power split device in a wind energy conversion system. The concept uses a planetary gearbox in order to split the generated power of a wind turbine between a synchronous generator and a permanent magnet synchronous machine. The synchronous generator is connected directly to the grid, while the permanent magnet synchronous machine is connected to the grid via a partial scale back-to-back converter. The investigation made in this paper mainly concerns the design and construction of an experimental setup capable of testing the feasibility of such a concept. The power split device is designed through the use of optimal power splitting. The experimental setup consists of a permanent magnet synchronous machine and a synchronous generator connected through the planetary gearbox harvesting the wind energy, emulated by an induction machine. As the synchronous generator is connected directly to the grid, the purpose of the permanent magnet synchronous machine is to keep the synchronous generator at grid frequency. Control of the permanent magnet synchronous machine is investigated using field oriented control and is tested using a numerical simulation.

Keywords: Power split device, Wind turbine, AC machine modelling, Field oriented control

1. Introduction

Wind energy is becoming a popular replacement for fossil fuel based power stations, creating issues with grid integrity, relating to the use of conventional wind energy conversion systems (WECS) and how they operate [2, 3].

Conventional WECSs used in the industry are defined as WECSs consisting of the doubly fed induction generator using a partial-scale power converter or WECSs with a permanent magnet synchronous generator using a full-scale power converter. The conventional WECSs are not directly coupled to the grid, creating issues with grid compliance during fault ride through. Extra measurements must be taken to ensure grid compliance. These might involve the use of external static compensators, ensuring grid stability in areas with high wind energy penetration. Others involve complicated control schemes, sometimes involving the wind turbine not operating at maximum efficiency or inducing increased mechanical stress and fatigue [4, 5, 6].

A concept seen in Fig. 1 of the WECS proposed by [1] may address some of these obstacles. The principle

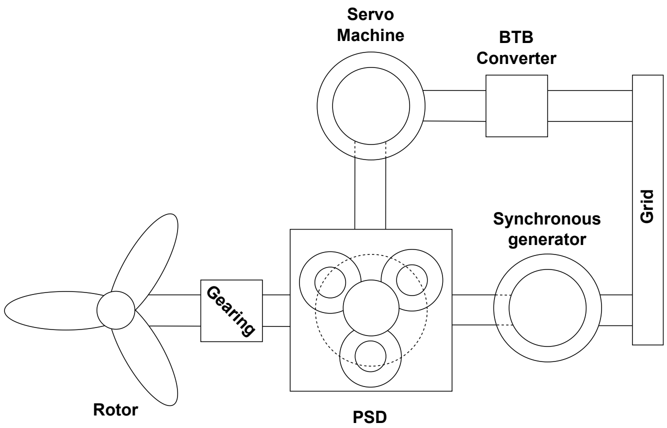

Fig. 1 PSD concept as proposed by [1]

of the concept is to use a power split device (PSD), to split the power from the wind turbine's rotor between a synchronous generator and a servo machine. The purpose of the servo machine is to keep the synchronous generator at grid frequency, by supplying or extracting power from the system. As a result, the synchronous generator is coupled directly to the grid, potentially allowing its system inertia to add grid stability [7].

In [1] and continued in [3], the PSD concept is investigated, providing examples of control and investigations towards the size of the power converter, needed to control the servo machine. Their work focuses on proving the concept of being able to maintain a synchronous speed under stochastic wind conditions. Further investigation is still needed to determine the fault ride through behaviour.

The aim of this paper is therefore to develop an experimental setup, that can be used to evaluate the PSD concept at Aalborg University.

2. Preliminary Studies

In order to use the experimental setup as a way to emulate a WECS using a PSD, it is needed to understand how wind turbines operate. Furthermore, a theoretical analysis using a wind turbine and WECS, with a PSD, forms the basis of initial design considerations for the setup.

2.1 Wind Turbine Characteristics

Understanding the dynamics of a wind turbine provides the basic information needed to construct a steady state turbine power curve.

The wind power absorbed by a wind turbine can be expressed as (1).

$$P_t = \frac{1}{2}\rho A C_P(\lambda, \beta) v_w^3 \tag{1}$$

Where $C_p(\lambda, \beta)$ is known as the power coefficient and is dependent on the pitch angle β and tip-speed ratio λ, defined as:

$$\lambda = \frac{\omega_t R_t}{v_w} \tag{2}$$

Where ω_t is the rotational speed of the turbine, and R_t is the turbine rotor radius.

An approximation of the power coefficient is presented by [8] as:

$$C_P = c_1 \left(\frac{c_2}{\lambda_i} - c_3\beta - c_4\beta^{c_5} - c_6 \right) e^{\frac{-c_7}{\lambda_i}} \tag{3}$$

Where c's represent turbine specific constants and λ_i is defined as:

$$\frac{1}{\lambda_i} = \frac{1}{\lambda + c_8\beta} - \frac{c_9}{\beta^3 + 1} \tag{4}$$

According to [9], (3) and (4) are not sufficiently accurate for modern turbines. The pitch angle β should instead be re-scaled as:

$$\beta' = c_{10}\beta \tag{5}$$

A conceptual steady state power curve of a wind turbine is constructed for use as a design basis, for the experimental setup. The steady state power curve used is that of a 2.5 MW turbine, with c's based on [9], as seen in Fig. 2.

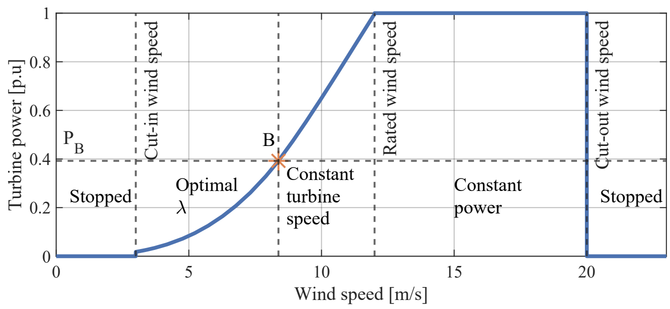

Fig. 2 Conceptual steady state power curve of a turbine, with respect to wind speed.

As seen in the figure the turbine is stalled, until the wind speed exceeds the cut-in wind speed. Increasing the wind speed further, the turbine will operate at an optimal tip-speed ratio, with the power coefficient remaining approximately constant.
Once the rated turbine speed is reached, the rotor blades will start to pitch, limiting the rotor speed. Having reached the rated wind speed, the pitch controller keeps the turbine at its rated speed and power. Finally, as the cut-out wind speed is reached, the turbine is shut down to avoid damaging the wind turbine [5].

2.2 Characteristics of a Power Split Device

To understand how a PSD operates when used in a wind turbine, a steady state model wherein the PSD is represented by a planetary gear set is made.

The steady state relations are derived using kinematic relations and Lagrangian mechanics. This deduces the dynamic relations, in which the transient parts are removed to obtain the steady state relations. The ring gear, carrier and sun gear are denoted with subscripts r, c, and s respectively. The steady state speed relation shows the relationship of the ring gear, carrier and sun gear speeds ω and is stated as (6) [1]:

$$(1 - i_0)\omega_c = \omega_s - i_0\omega_r \tag{6}$$

Where i_0 is a ring gear to sun gear ratio referred to as the characteristic ratio, which is defined as:

$$i_0 = -\frac{r_r}{r_s} = -\frac{Z_r}{Z_s} \tag{7}$$

Where r is the radius and Z is the number of teeth. This gear ratio typically ranges from -9 to $-3/2$ [10].

Considering a frictionless PSD, the steady state torque (T) relations can be derived to be:

$$T_s + T_c + T_r = 0 \tag{8a}$$

$$\frac{r_p}{r_r} T_r - \frac{r_p}{r_s} T_s = 0 \tag{8b}$$

These two equations can be combined and rewritten to include i_0, which results in the following two equations:

$$T_s = -\frac{1}{1 - i_0} T_c \tag{9a}$$

$$T_r = \frac{i_0}{1 - i_0} T_c \tag{9b}$$

Having derived the equations necessary to describe steady state of the PSD, the equations can be used to determine the optimal power splitting for the PSD when used in a wind turbine.

2.3 Optimal Power Splitting

[1] has developed an analytical method to optimise power splitting for a given power curve, by using the presented models above. [1] defines the main gearbox ratio as:

$$\frac{\omega_{turbine}}{\omega_{mainshaft}} = xG_0 \tag{10}$$

Where G_0 is a constant defined as:

$$G_0 = \frac{\omega_{turbine.rated}}{\omega_1} \tag{11}$$

Where ω_1 is the synchronous speed of the generator, and x is a scalar value that is determined to achieve optimal power splitting. Furthermore, [1] defines variants of the PSD concept as seen in Table I.

Tab. I Possible variants of a PSD WT

Variant	Main shaft	Syn. Generator	Servo machine
A	Carrier	Sun gear	Ring gear
B	Carrier	Ring gear	Sun gear
C	Sun gear	Carrier	Ring gear
D	Sun gear	Ring gear	Carrier
E	Ring gear	Carrier	Sun gear
F	Ring gear	Sun gear	Carrier

For all variants the minimum power ratio of the servo machine ($P_{servo}/P_{turbine.rated}$), is dictated by the characteristic power ratio of the power curve b, which is defined in [3] as (12):

$$b = \frac{P_B}{P_{turbine.rated}} \tag{12}$$

Where P_B is the turbine power at point B, as illustrated in Fig. 2 and $P_{turbine.rated}$ is the rated power of the turbine. The optimal power splitting can then be calculated by solving the following equation for a [1]:

$$1 - a_{opt} = \frac{4}{27} b a_{opt}^3 \tag{13}$$

Where a is defined according to Table II [1].

Tab. II a definition for all variants

Variant	a definition
A	$\frac{1}{(1-i_0)x}$
B	$-\frac{i_0}{(1-i_0)x}$
C	$\frac{1-i_0}{i_0 x}$
D	$-\frac{i_0}{i_0 x}$
E	$-\frac{1-i_0}{i_0 x}$
F	$-\frac{1}{i_0 x}$

Calculations of the speed and torque requirements for all variants can be calculated as seen in Table III, where $\Delta\omega$ is the normalised speed variation of the main shaft using synchronous speed ω_1 as base value:

$$\Delta\omega = \frac{\omega_{mainshaft}}{\omega_1}, \{\Delta\omega \in \mathbb{R} \| -1 \leq \Delta\omega \leq 0\} \tag{14}$$

Synchronous speed ω_1 is the synchronous speed of the generator assuming no gearing between the generator and PSD. T_c^* is the torque acting on the carrier with $x = 1$ [1].

Tab. III Speed and torque of the servo machine for different variants [1]

Variant	Servo speed ω_{servo}	Servo torque T_{servo}
A	$-\frac{\omega_1(1-a+\Delta\omega)}{i_0 a}$	$-a i_0 T_c^*$
B	$-\frac{i_0\omega_1(1-a+\Delta\omega)}{a}$	$-\frac{a}{i_0} T_c^*$
C	$-\frac{(1-i_0)\omega_1(1-a+\Delta\omega)}{i_0 a}$	$-\frac{a i_0}{1-i_0} T_c^*$
D	$-\frac{i_0\omega_1(1-a+\Delta\omega)}{(1-i_0)a}$	$-\frac{a(1-i_0)}{i_0} T_c^*$
E	$\frac{(1-i_0)\omega_1(1-a+\Delta\omega)}{a}$	$\frac{a}{1-i_0} T_c^*$
F	$\frac{\omega_1(1-a+\Delta\omega)}{(1-i_0)a}$	$a(1-i_0) T_c^*$

The power curve shown in Fig. 2 is found to have an optimal a value of $a_{opt} \approx 0.95$ using (13). The power

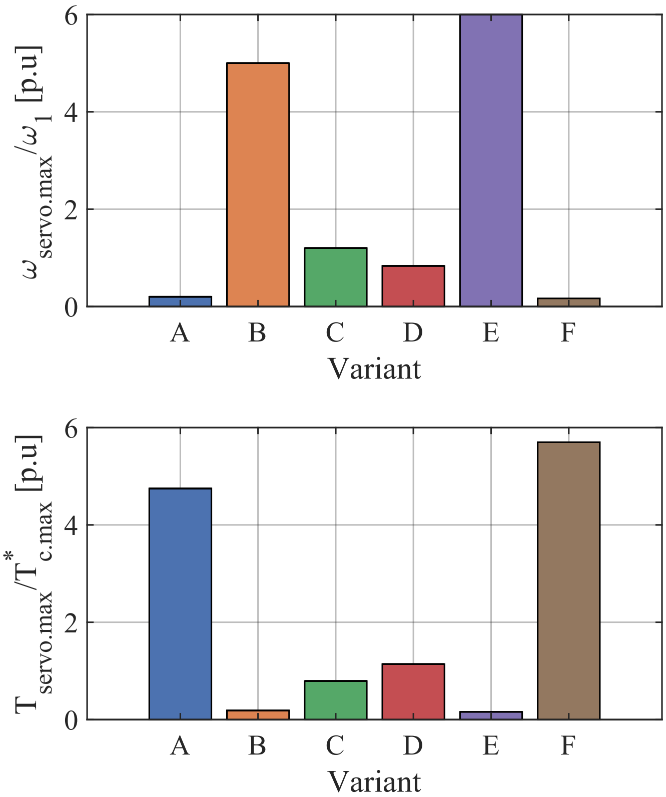

Fig. 3 Speed and torque requirements for all variants

and speed requirements based on a characteristic gearing of $i_0 = -5$, can be seen in Fig. 3.

As seen in Fig. 3 only the B and E variant are viable options for a configuration, as the torque is deemed too high for other variants.

For the experimental setup, a B variant is therefore chosen, based on available resources, as a basis for the design.

3. Design of Experimental Setup

In the B variant, the synchronous generator is connected to the ring gear. In order for the ring gear not to operate at high speeds, gearing is introduced. Furthermore, an induction motor is used to emulate the main shaft containing the wind turbine rotor and main gearing.

The setup is scaled to follow the power characteristics presented in Fig. 2, by scaling the torque. The torque scaling factor is calculated as stated in (15).

$$K_{scaling} = \frac{P_{setup}}{P_{turbine.rated}} \tag{15}$$

An overview of the B variant setup, with the induction motor emulating the wind turbine, and the gearing between the ring gear and synchronous generator is sketched in Fig. 4.

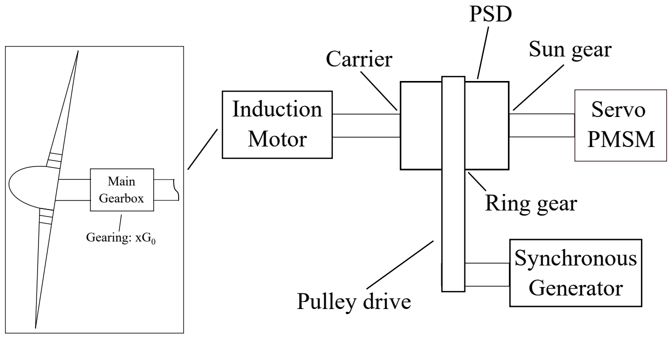

Fig. 4 Sketch of the experimental setup

A setup is designed based on the above concept, where some parts are designed and manufactured in-house while others are chosen based on available standard parts. Some parts are predetermined, such as the permanent magnet synchronous machine (PMSM) chosen as the servo machine, and the planetary gear set used. A model showing the different components of the designed experimental setup is seen in Fig. 5.

3.1 Implementation of Setup Controller

Having designed and sketched the mechanical parts needed to construct the setup, the implementation of control in the setup is investigated. The setup consists of three different AC machines, where one of them is a synchronous generator, hence no control is needed. For the induction machine to emulate the wind turbine, a variable frequency drive can be used since the induction machine only needs to operate as a motor. The servo machine needs to operate both as a motor and a generator, hence it is connected to an evaluation board. The main components of the evaluation board are an inverter to supply the PMSM with power and a microcontroller (µC) to control the inverter signals to the PMSM. The inverter is a 2-level inverter utilising 6 insulated-gate bipolar transistors to produce 3-phased power signals. The power signals are produced through the µC using space vector pulse width modulation (SVPWM). The SVPWM method is chosen since the method can achieve a phase-to-phase voltage that is 15% higher than the DC input and a reduction in torque ripples because of the general reduction in total harmonic distortion [11].

Furthermore, the setup consists of a computer used both as a terminal to communicate with the µC via a universal asynchronous receiver/transmitter (UART) and a debugging environment to debug via an integrated development environment. The electronic setup is seen in Fig. 6.

The PMSM is modified with an incremental encoder instead of its original resolver as the evaluation board

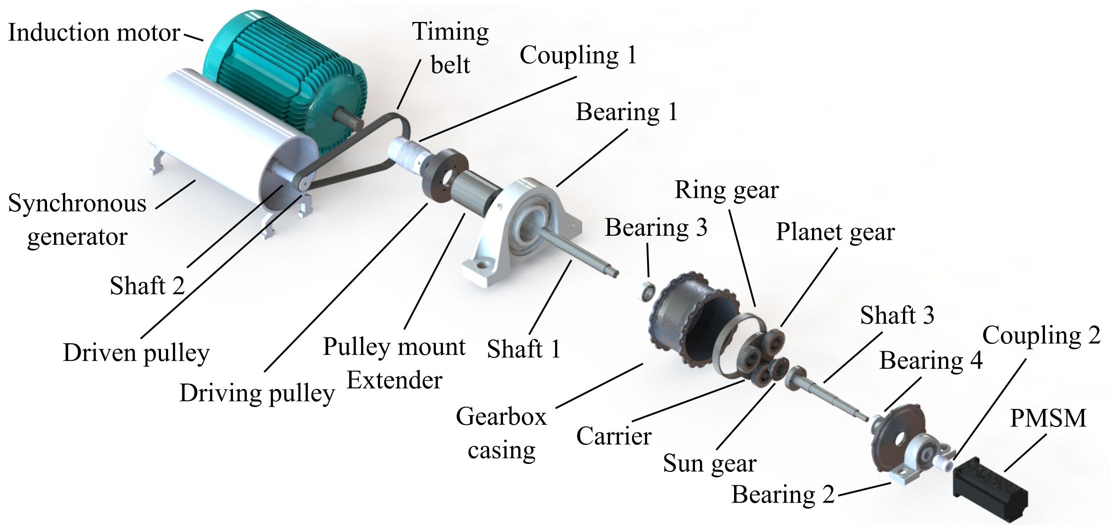

Fig. 5 Overview of sketched experimental setup using given components

is only compatible with an incremental encoder. An incremental encoder is not absolute, as such an alignment procedure is added to calibrate the encoder to a fixed starting point. The encoder can be used for data capture, model validation, and speed control of the PMSM.

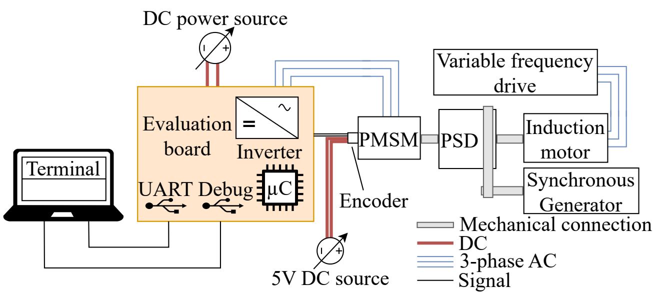

Fig. 6 An overview of the experimental setup's wiring and connections with the µC. Different colours signify different types of power along with the signal wires.

4. Modelling and control of PMSM

The governing differential equations are two current equations and Newton's II law as seen in (16). The PMSM used in the setup is a surface-mounted PMSM, which makes the d and q-axis inductance equal hence $L_q = L_d = L$.

$$\frac{d}{dt}i_d = \frac{1}{L_d}v_d + \frac{L_q p}{L_d}\omega_r i_q - \frac{R_s}{L_d}i_d \tag{16a}$$

$$\frac{d}{dt}i_q = \frac{1}{L_q}v_q - \frac{L_d p}{L_q}\omega_r i_d - \frac{R_s}{L_q}i_q - \frac{p\lambda_f}{L_q}\omega_r \tag{16b}$$

$$\frac{d}{dt}\omega_r = \frac{1}{J}\left(\tau_e - \tau_m - B\omega_r\right) \tag{16c}$$

where v_d and v_q are the direct and quadrature axis voltages, p is the total number of pole pairs, ω_r is the mechanical speed, R_s the stator resistance per phase, λ_f is the permanent magnet flux linkage, J is the inertia, τ_e is the electromagnetic torque and τ_m is the torque applied to the machine.

The electromagnetic torque is found as:

$$\tau_e = \frac{3p}{2}\left(\lambda_f i_q + (L_d - L_q)i_d i_q\right) \tag{17}$$

Fig. 7 shows how Field oriented control (FOC) is implemented in the control of the PMSM. The feedforward compensation consists of the coupled terms of (16), shown in (18).

$$v_{d,ff} = \frac{pL_q}{L_d}\omega_r i_q \tag{18a}$$

$$v_{q,ff} = \frac{pL_d}{L_q}\omega_r i_d + \frac{p\lambda_f}{L_q}\omega_r \tag{18b}$$

If the currents and motor speed are measured perfectly the transfer function from current to electromagnetic torque approximates to (19).

$$G_{P.c}(s) = \frac{1}{Ls + R_s} \tag{19}$$

Using pole zero cancellation the current controllers are determined in (20).

$$K_{P.c} = L\omega_c \tag{20a}$$

$$K_{I.c} = R_s\omega_c \tag{20b}$$

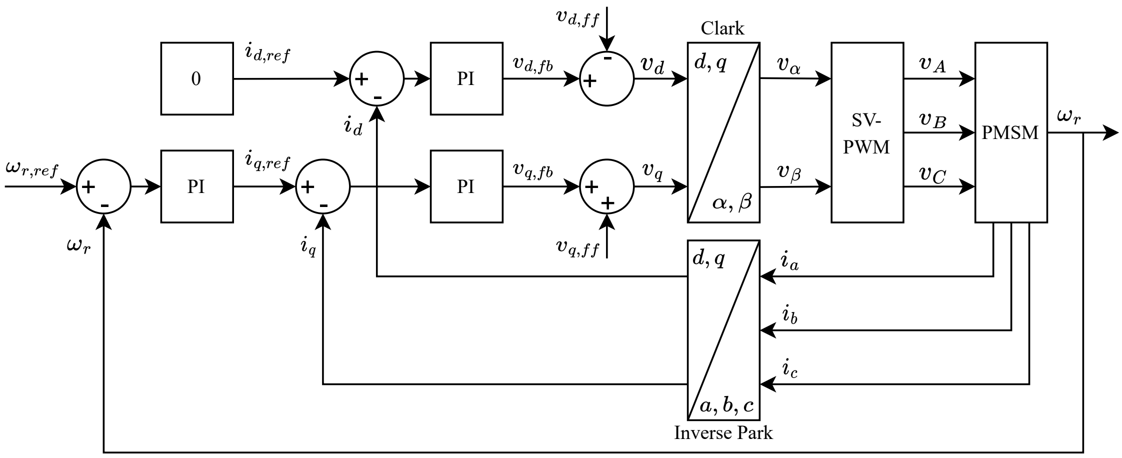

Fig. 7 Block diagram of servo PMSM control system

Where ω_c is the bandwidth of the current loops, chosen to be 1/20 of the switching frequency of the µC. From (17) it is seen that only the q-axis current generates torque if the inductances are equal. This leads to a desired d-axis current of zero.

A step is given for the q-axis current while the d-axis current's reference is kept constant at zero. The simulated results are seen in Figs. 8 and 9 showing the q-axis current stepping to one ampere and the d-axis current remaining at zero respectively.

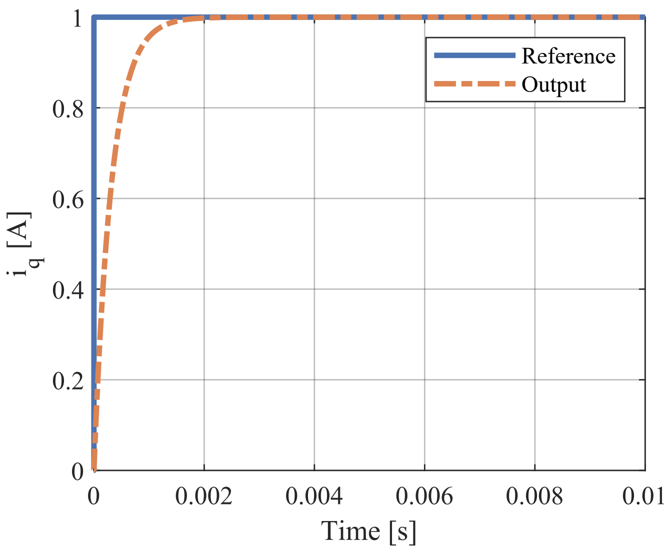

Fig. 8 Response for i_q when given step input with unit amplitude

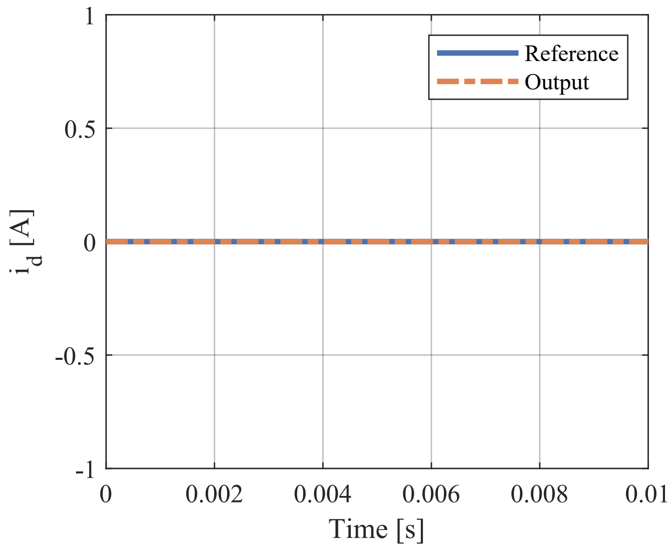

Fig. 9 Response for i_d when given constant input with zero amplitude

Assuming that the current controller is sufficiently fast it can be modelled as a unity gain, making the transfer function from q-axis voltage to mechanical speed, derived from (16c):

$$G_s(s) = \frac{\frac{3p\lambda_f}{2J}}{s + \frac{B}{J}} \tag{21}$$

A controller is chosen based on a desired bandwidth of the speed loop of 1/5 of the current loops' bandwidth. The chosen control parameters are shown in (22).

$$K_{P.s} = 0.067 \tag{22a}$$

$$K_{I.s} = 0.01 \tag{22b}$$

The closed-loop step response in both directions, of the linear and the nonlinear model is shown in Fig. 10

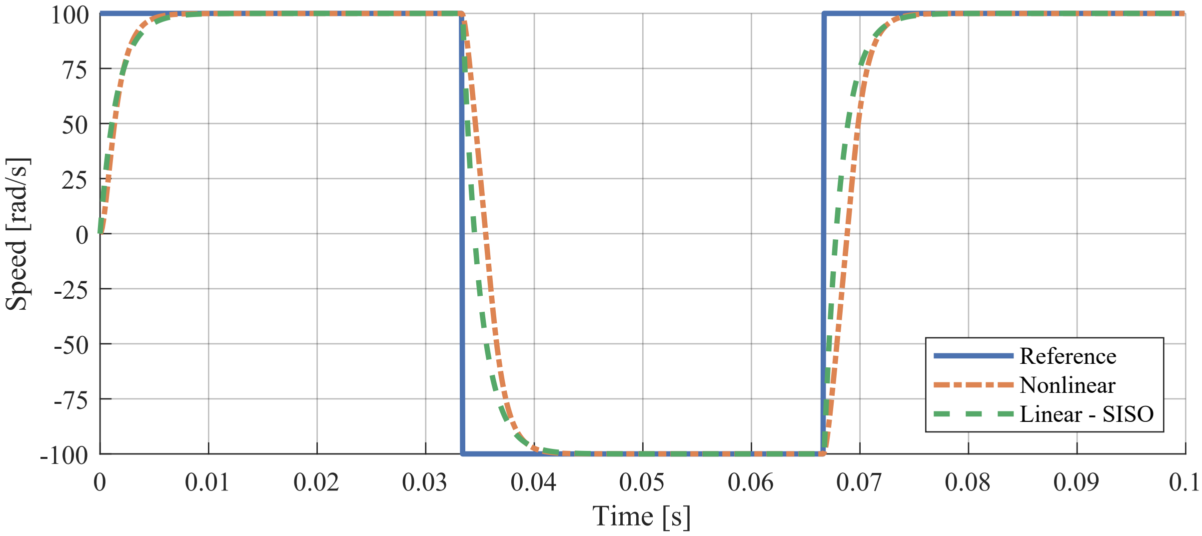

Fig. 10 Closed-loop step response

Its behaviour is approximately that of a first-order system, which indicates that the inner current control loops are performing as expected. And the similarity between the linear and nonlinear models indicates that (21) is an acceptable approximation to the nonlinear system. A further discussion of the models and the experimental setup is seen in the next section.

5. Discussion

The modelling, simulation and control consider the PMSM in isolation. To investigate the performance of the controllers designed, a model of the entire setup should be included. This should be done to include different system behaviours, changing the order of the system used for simulating, and introducing new nonlinearities. Thus the controller requirements would be dictated by the whole system.

The SVPWM signals are chosen to be excluded in order to keep the calculation time low. The exclusion is assumed to have a negligible impact on the shown results, as directly using the reference would approximately be equal in a simulation environment.

The decoupling terms in the control scheme consist of the mechanical speed ω_r and the currents which are fed back to the controller. The mechanical speed is read by an incremental encoder which introduces noise to the system, and in turn, makes the decoupling terms inaccurate. Thus the assumption of no d-axis current becomes invalid. The effect of this has to be tested to examine its significance. A low-pass filter can be utilised to accommodate noise problems.

Modelling and control are made based on the designed experimental setup, which is a linearly scaled approximation of an industrial wind turbine based on its torque scaling factor $K_{scaling}$. Whereas in reality not all behaviours may be scaled linearly, such as frictional losses. It is however expected that the setup is capable of producing results which can be used to determine the feasibility and behavioural patterns of the concept since the principles for the scaled setup and a fully scaled concept are the same.

6. Conclusion

In conclusion, an experimental setup is successfully designed and constructed to test the feasibility of a WECS utilising a PSD, based on a scaled WT model.

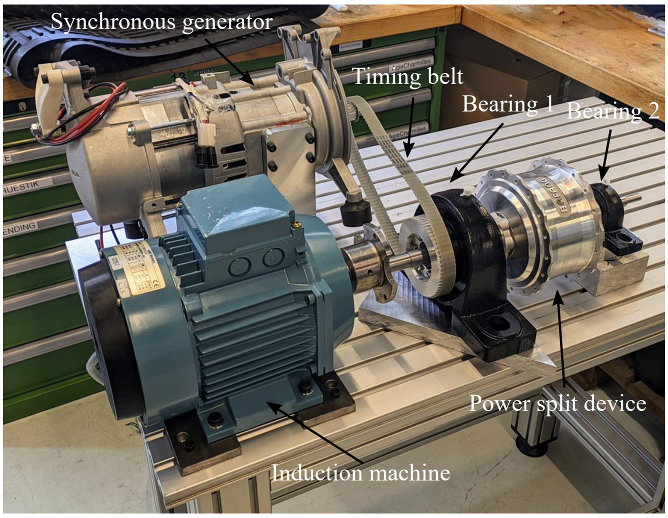

Fig. 11 Picture of the constructed experimental setup without the PMSM and electrical components

The constructed experimental setup without the PMSM and electrical components is seen in Fig. 11.
Control of the setup is implemented through the use of a μC and SVPWM. A FOC scheme is designed for the setup based on the modelling of a PMSM.

Acknowledgement

The authors of this work gratefully acknowledge Grundfos for sponsoring the 11th MechMan symposium.

References

[1] Q. Liu, R. Appunn, and K. Hameyer, "A study of a novel wind turbine concept with power split gearbox," *Journal of international Conference on Electrical Machines and Systems*, vol. 2, no. 4, pp. 478–485, 2013.

[2] J. Hossain and H. R. Pota, *Robust Control for Grid Voltage Stability: High Penetration of Renewable Energy*. Springer, 2014.

[3] Q. Liu, R. Appunn, and K. Hameyer, "Wind turbine with mechanical power split transmission to reduce the power electronic devices: An experimental validation," *IEEE transactions on industrial electronics (1982)*, vol. 64, no. 11, pp. pp.8811–20, 2017.

[4] X. Yan and X. Sun, "Inertia and droop frequency control strategy of doubly-fed induction generator based on rotor kinetic energy and supercapacitor," *Energies (Basel)*, vol. 13, no. 14, pp. 3697–, 2020.

[5] V. Yaramasu and B. Wu, *Basics of Wind Energy Conversion Systems (Wecs)*, pp. 1–60. John Wiley & Sons, Inc., 2017.

[6] A. D. Hansen, N. A. Cutululis, H. Markou, P. Sørensen, and F. Iov, "Grid fault and design-basis for wind turbines - final report," Tech. Rep. ISBN: 978-87-550-3789-2, Risø DTU, P.O.Box 49 DK-4000 Roskilde, January 2010.

[7] P. M. Anderson and A. A. Fouad, *Power System Control and Stability*. IEEE Press, 1994.

[8] S. Heier, *Grid integration of wind energy conversion systems.* Chichester: John Wiley & Sons, 2nd ed. ed., 2006.

[9] J. Fortmann, *Modeling of wind turbines with doubly fed generator system*. Springer, 2014.

[10] V. Vullo, *Gears Volume 1: Geometric and Kinematic Design*. Springer Series in Solid and Structural Mechanics, 10, Cham: Springer International Publishing, 1st ed. 2020. ed., 2020.

[11] M. H. Rashid, *Power Electronics: Devices, Circuits and Applications*, ch. 6. Harlow: Pearson, 4. ed., international edition. ed., 2014.